Earth and Planetary Science Letters 391 (2014) 263–273

Contents lists available at ScienceDirect

Earth and Planetary Science Letters

www.elsevier.com/locate/epsl

Newly-formed illite preserves fluid sources during folding of shale and limestone rocks; an example from the Mexican Fold-Thrust Belt

Elisa Fitz-Díaz [a,b,*], Antoni Camprubí [b], Edith Cienfuegos-Alvarado [b], Pedro Morales-Puente [b], Anja M. Schleicher [a], Ben van der Pluijm [a]

[a] Department of Earth & Environmental Sciences, University of Michigan, 1100 North University Ave., Ann Arbor, MI 48109-1005, United States
[b] Instituto de Geología, Universidad Nacional Autónoma de México, Ciudad Universitaria, 04510 México DF, Mexico

ARTICLE INFO

Article history:
Received 24 May 2013
Received in revised form 25 October 2013
Accepted 16 December 2013
Available online xxxx
Editor: G.M. Henderson

Keywords:
illite
folds
veins
fluid inclusions
water
stable isotopes

ABSTRACT

We combine structural, fluid-inclusion microthermometry, illite-crystallinity, X-Ray Diffraction (XRD) and O and H stable isotope analyses of authigenic illite to determine the source of local fluids interacting with rock during folding in anchizonal shales of the Mexican Fold-Thrust Belt (MFTB). A well-exposed train of mesoscopic, asymmetrical folds in a sequence of Cretaceous limestones interbedded with shale was targeted for this study. We test the hypothesis that syn-folding vein minerals and clay minerals were formed from the same fluids by comparing the δ^2H composition of inclusion fluids in calcite and quartz from veins, and from illite concentrates from sheared shale layers, and the sources of that fluid.

Five clay size-fractions (<0.05, 0.05–0.2, 0.2–1, 1–2, and <2 μm) were separated from eight shale samples. In the 40 clay grain-size fractions analyzed, illite, calcite, kaolinite, smectite, chlorite and minor quartz were identified by XRD analysis. Most samples show different proportions of various clay minerals, except for the finer fractions in two of the samples (BL3 and BL4) were illite is the only clay phase present. The discriminating potential of δ^{18}O values of clay is generally masked by the abundance of calcite in all samples. In contrast, samples containing chlorite and smectite show very low values in δ^2H (−75.9 to −53.9‰), while samples containing illite and kaolinite or pure illite show relatively high δ^2H values (−33.1 to −50.1‰). The latter fall within the δ^2H range (−39 to −49‰) determined in fluid inclusions of syntectonic veins, indicating isotopic equilibrium between water, veins fillings and illitic clay during deformation, according to fractionation factors at these temperatures (220–250 °C). The δ^2H values and fluid inclusion salinities in the sampled rocks indicate that water active during folding was partly marine and partly meteoric and that the amount of such pore-water represented a small fraction of the deformed rock volume. Our study demonstrates that the H-isotopic composition of anchizonal illitic clays, commonly present in exhumed fold-thrust belts, can be used to determine the source(s) of fluids that were active during deformation.

1. Introduction

Fluids play an essential role in the evolution of sedimentary sequences into fold-thrust belts by means of facilitating fracturing and/or faulting on a range of scales (*e.g.*, Hubbert and Rubey, 1959; Ramsay, 1967; Engelder, 1984; Fyfe and Kerrich, 1985; Hudleston, 1989; Cosgrove, 1993; Bjørlykke, 1997; Sibson, 1997; Anastasio et al., 2004; Evans and Fischer, 2012) and by supporting chemical reactions during pressure-solution and material transfer processes (*e.g.*, Durney, 1972; Rutter, 1983) within the rock volume. These processes commonly involve soluble materials at low temperatures, such as calcite and quartz, as well as the coeval formation of clay minerals (Marshak and Engelder, 1984; Eslinger and Yeh, 1986; Ferket et al., 2003; Hilgers et al., 2006). Numerous studies based on comparative geochemical, structural and fluid inclusion analyses of syntectonic veins that were formed in folded layers or thrust zones, have allowed an understanding of fluid circulation, and constraining pressure and temperature conditions during deformation (Rye and Bradbury, 1988; Foreman and Dunne, 1991; Hodgkins and Stewart, 1994; Kirschner and Kennedy, 2001; Richards et al., 2002; Travé et al., 2007; Fitz-Díaz et al., 2008; Lacroix et al., 2011). The source of fluids active during deformation of sedimentary sequences has been mostly investigated by means of carbonate geochemistry and microthermometry of fluid inclusions trapped in calcite and quartz of syntectonic veins (Fischer et al., 2009; Fitz-Díaz et al., 2011; Evans et al., 2012; Lacroix et al., 2012). The formation of authigenic illite is well documented in basinal sequences and fold-thrust belts at very low metamorphic grade (see Merriman and Frey, 1999, and references therein), and fractionation factors of H and O isotopes between water and illite or illite/smectite have been investigated

* Corresponding author.
E-mail address: fitzdiaz@umich.edu (E. Fitz-Díaz).

0012-821X/$ – see front matter
http://dx.doi.org/10.1016/j.epsl.2013.12.025

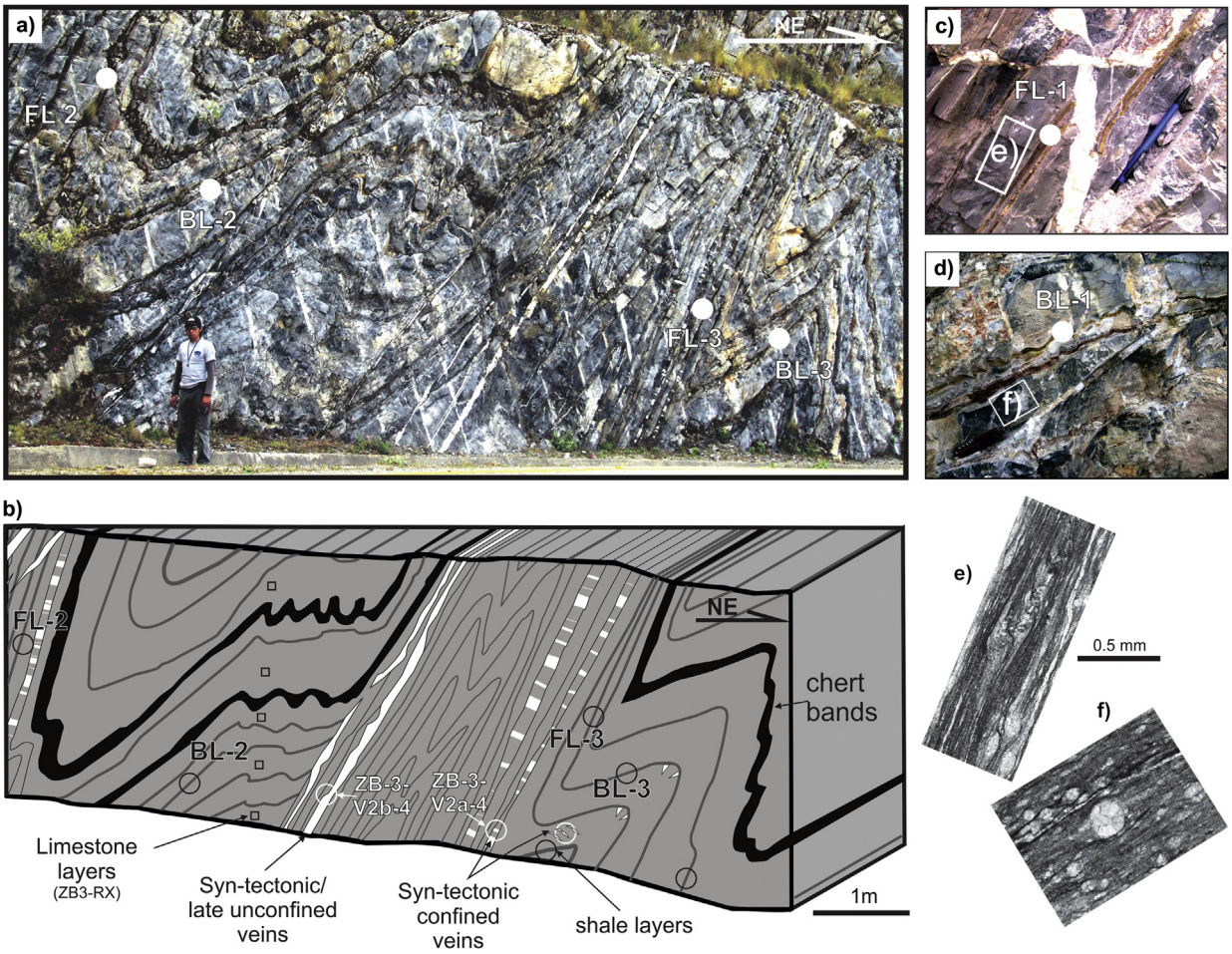

Fig. 1. The studied rocks of the Zimapán Basin of the Mexican Fold-Thrust Belt. (a) Road cut exposure of folded limestone layers interbedded with chert bands and shale layers. (b) Schematic representation of the asymmetrical folds, showing attenuation in the forelimb of folds, the distribution of syntectonic veins in dilation areas around the fold and spots where some samples were collected for analysis of water trapped in fluid inclusions (white circles), clays from shale layers (black circles) and limestone layers (black squares). To the right, photographs (c) and (d) show close-ups to sites FL1 and BL1 sampled in this study in an asymmetrical fold to the right of those in (a) but part of the same train. Below (c) and (d), photomicrographs in (e) and (f) show evidence of strong internal deformation within the limestone layers, evidenced by distortion of calcispherulid shells. The abundance of stylolites and pressure-solution seams suggests material transfer as a main deformation mechanism in these rocks.

over the last four decades (Savin and Epstein, 1970; James and Baker, 1976; Eslinger et al., 1979; Yeh, 1980; Capuano, 1992; Sheppard and Gilg, 1996; Chacko et al., 2001; Hyeong and Capuano, 2004). However, only few studies use H and/or O stable isotopes from illite and illite–smectite to track the origin of the fluid from which they precipitated (Eslinger and Yeh, 1986; Compton et al., 1999). This paucity is due to several reasons, including: (1) it is difficult to separate pure illitic clay from rocks because their small grain size (<2 μm) complicates physical separation from other phases and chemical separation can alter isotopic compositions, (2) oxygen is present in calcite and quartz, which are commonly found in association with clay minerals in sedimentary rocks, thus rendering interpretation of $\delta^{18}O$ of clays difficult, (3) hydrogen, in contrast, is a main component of clay minerals and is not present in other common minerals of shale (*e.g.*, calcite, quartz and hematite), except that organic matter present can affect the isotopic composition of clay minerals, (4) the amount of structural water (OH in octahedral layers) in discrete illite is small compared to atmospheric water that can be adsorbed on the clay surface area during sample preparation, producing significant isotopic shifts during measurements, so careful sample preparation (water extraction in a vacuum line or fast drying and packing) is necessary, and (5) discrepancies in fractionation factors of ^{2}H between illite/smectite and water reported in the literature (*e.g.*, Yeh, 1980; Capuano, 1992) can complicate the application of $\delta^{2}H$ analysis to constrain the source of fluid.

Given the importance of knowledge of fluid sources for a range of geologic phenomena and to examine whether illite is able to preserve the signature of fluids, we analyzed different size-fractions of clays in eight shale samples from a continuously-exposed sequence of multilayer, mesoscopic chevron folds. These folds were the result of flexural slip/flow (Ramsay, 1967; Hudleston, 1989) with associated veining in the hinges and attenuated forelimbs, and a strong shear parallel to bedding in bentonitic shale layers, but also evident in limestone layers by thickness variations and distortions of calcispherulids shelves on the microscopic scale (Fig. 1). Fluids provided the means for pressure-solution and material transfer during folding, allowing stylolite formation and vein precipitation within limestone layers and illite growth in shale layers. The isotopic signature of authigenic illite-bearing shale should be in agreement with that of water trapped in fluid inclusions of syntectonic veins at the temperature of deformation, using the fractionation factor of Capuano (1992) for temperatures >200 °C. In previous work (Fitz-Díaz et al., 2011) a well-constrained range of $\delta^{2}H$ values for water from primary and pseudosecondary fluid inclusions trapped in syntectonic veins was determined. Temperatures of homogenization (160 to 190 °C) were also obtained from these fluid inclusions, which, after pressure correction (Goldstein and Reynolds, 1994), provided

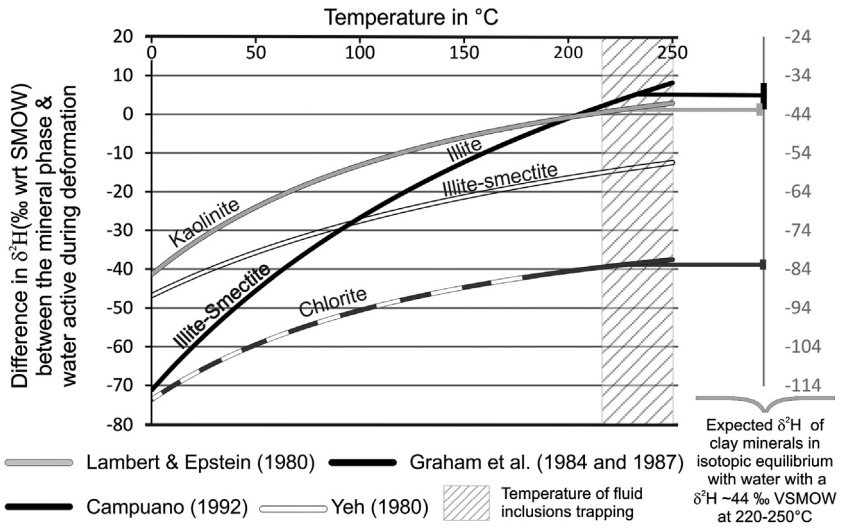

Fig. 2. Correlation between temperature and difference in δ^2H values for illite/smectite–illite, kaolinite and chlorite, based on fractionation factors reported in the literature. This plot predicts isotopic compositions of clays in equilibrium with water at a given temperature. On the right side of the figure we show the predicted compositions for clays in the analyzed outcrop, based on a temperature of deformation of 225–250 °C, and $\delta^2\text{H} = -44‰$ wrt VSMOW for water active during deformation.

temperatures of trapping between 220 and 250 °C. With this information we adopt the fractionation factor for hydrogen between structural water (which excludes water in smectite interlayers) in illite/smectite and pore water of Capuano (1992) over that of Yeh (1980), from which different results would be obtained (Fig. 2). The fractionation factor of Capuano (1992) takes into account samples below the uppermost 3 kilometers from the Gulf Coast basin, in which illite is poorly crystalized and is interlayered with smectite, and samples that experienced geopressurized conditions (more than 3 km of cover) where discrete illite prevails (see Hyeong and Capuano, 2004, for further discussion). The shale layers targeted in this study contain discrete illite as the dominant phase and were similarly exposed to geopressurized conditions, as indicated by the abundance of veins confined within and among layers. Whereas kaolinite, chlorite, and smectite are also present in different proportions in some of the samples, we target discrete illite as the main focus of this study, because Ar/Ar ages of illite from a sample in this outcrop demonstrate that it grew during deformation (Fitz-Díaz et al., in press).

We test if discrete illite satisfies predicted values from the fractionation factor of Capuano (1992), by considering the composition of water active during deformation (trapped in fluid inclusions) and the temperature range of deformation. Then, we examine the implications of the measured isotopic compositions in terms of fluid origin (i.e., metamorphic, formational, meteoric), fluid budget and fluid circulation within the folded carbonate horizons of the evolving fold-thrust wedge.

2. The studied outcrop

The train of mesoscopic asymmetrical chevron folds studied in this paper is well-exposed and involves a sequence of 20–50 cm thick limestone layers interbedded with thin layers of bentonitic shale and chert bands of the Tamaulipas Formation, which is the characteristic unit of the Cretaceous Zimapán Basin in central eastern Mexico (Suter, 1987; Fig. 1a). The folds are roughly oriented NW–SE and have axial planes and cleavage/stylolites that dip steeply to the SW (Fitz-Díaz et al., 2012), and show attenuated forelimbs compared to backlimbs. This geometry mimics the general orientation of the Zimapán Basin and is consistent with SW–NE directed shortening. The sedimentary sequences in the Zimapán Basin consist of about 800–1200 m of Cretaceous basinal carbonate rocks, where 300–500 m of those correspond to the Tamaulipas Formation. This basin was confined between two relatively rigid carbonate platforms during deformation and accommodated about 60% shortening, dominantly by folding and by pressure solution and material transfer (Fitz-Díaz et al., 2012). No major thrusts or reverse stratigraphic offsets have been recognized within the basin.

Prior studies that were carried out in this outcrop provided relevant information to the present study. δ^{13}C and δ^{18}O comparative analyses in calcite from syntectonic veins and host rock showed identical isotopic values (Table 1), thus indicating that most of the vein calcite was derived from the host rocks through extensive fluid–rock interaction between limestone and water, and/or the possibility that a limited amount of non-formational water was involved in the deformation of these rocks (Fitz-Díaz et al., 2011). δ^2H analyses of water trapped in primary and pseudo-secondary fluid inclusions gave an average δ^2H value of $\sim -44 \pm 5‰$ for the water active during deformation, which is very similar among the four samples collected across the outcrop (Table 1, Fig. 1b). Microthermometry of fluid inclusions in these veins indicated that they belong to the H_2O–NaCl system, with salinities that range between 8 and 9 wt.% NaCl equivalent, and no other fluids present. Temperature of deformation varies between 220 and 250 °C. Lastly, Ar–Ar geochronology of the same clay size-fractions used from sample FL1 in this study (sample SZ3-FL in Fitz-Díaz et al., in press) shows that these minerals precipitated during deformation in the Late Cretaceous (76.5 ± 1.0 Ma).

3. Methods

We combine existing isotopic and microthermometric studies in fluid inclusions from veins (Fitz-Díaz et al., 2011) to examine if illitic clays preserve the same isotopic composition of water during deformation. For this purpose we centered our analysis on 4 samples collected in the forelimb (FL samples) and 4 samples in the backlimb (BL samples, Table 2) of asymmetrical folds in outcrop, matching sample locations of previously analyzed veins (Fig. 1b). We collected 300 grams of shale samples in both limbs to test if strain history or disposition/dip of the layers has an effect on mineralogical variations and/or isotopic compositions. In these samples, five different size-fractions were separated by centrifugation, to separate illite from other phases in the different size-fractions, to obtain isotopic signatures of illite.

Table 1
Stable isotope data measured in calcite and water sources used in the present analysis. On the left, $\delta^{13}C$ and $\delta^{18}O$ measured in calcite from limestone layers and syntectonic veins, and $\delta^{2}H$ measured in water trapped in fluid inclusions in calcite and quartz. Some of this water was extracted from calcite at 400 °C at once or in 100 °C steps of heating (these data were previously reported in the Annex of Fitz-Díaz et al., 2011). VSMOW = normalized with the Vienna Standard Mean Ocean Water; PDB = normalized with the Pee Dee Belemnite standard.

Sample	Material analyzed	$\delta^{13}C$ (‰) PDB	$\delta^{18}O$ (‰) VSMOW	$\delta^{2}H$ (‰) VSMOW
ZB3-R1	Platformal limestone	2.55	26.33	
ZB3-R2	Basinal limestone	2.94	26.42	
ZB3-R3	Basinal limestone	3.17	26.42	
ZB3-R4	Basinal limestone	3.2	26.42	
ZB3-R5	Basinal limestone	3.4	26.42	
ZB3-R6	Calcite from syntectonic vein	3.3	26.42	
ZB3-V2a-4	Calcite from syntectonic vein emplaced in chert band on attenuated limb	3.15	26.42	
H_2O from fluid inclusions in calcite step heated at 200 °C				−57.3
H_2O from fluid inclusions in calcite step heated at 300 °C				−44.6
H_2O from fluid inclusions in calcite step heated at 400 °C				−42.8
H_2O from fluid inclusions in quartz heated at 200 & 300 °C				NF
H_2O from fluid inclusions in quartz step heated at 400 °C				−59.5
H_2O from fluid inclusions in quartz step heated at 500 °C				NF
H_2O from fluid inclusions in quartz step heated at 600 °C				44.2
ZB3-V2a-5	Calcite and quartz from syntectonic vein emplaced within a chert band	3.98	26.03	
H_2O from fluid inclusions in calcite decrepitated at 400 °C				−45.62

Sample	Material analyzed	$\delta^{13}C$ (‰) PDB	$\delta^{18}O$ (‰) VSMOW	$\delta^{2}H$ (‰) VSMOW
ZB3-V2b-4	Calcite from unconfined vein parallel to late thrusts/shear zones	3.10	26.22	
H_2O from fluid inclusions in calcite decrepitated at 400 °C				−46.1
H_2O from fluid inclusions in calcite step heated at 200 °C				−61.9
H_2O from fluid inclusions in calcite step heated at 300 °C				−45.4
H_2O from fluid inclusions in calcite step heated at 400 °C				−41.8
ZB3-V2b-5	Calcite from calcite vein emplaced within limestone layers during folding	4.12	26.21	
H_2O from fluid inclusions in calcite decrepitated at 400 °C				−40.1
H_2O from fluid inclusions in calcite step heated at 200 °C				NF
H_2O from fluid inclusions in calcite step heated at 300 °C				−43.5
H_2O from fluid inclusions in calcite step heated at 400 °C				NF
ZB1-V2-5	Calcite from synfolding vein	1.5	26.9	
H_2O from fluid inclusions in calcite decrepitated at 400 °C				−41.9
ZB2-V2A-5	Calcite from synfolding vein	3.62	25.92	
H_2O from fluid inclusions in calcite decrepitated at 400 °C				−43.25
ZB2-V2B-5	Calcite from synfolding vein	3.41	25.62	
H_2O from fluid inclusions in calcite decrepitated at 400 °C				−45.3

Data used to constrain the $\delta^{2}H$ of −44±5‰ wrt VSMOW for pore water active during deformation.

$\delta^{2}H$ of water extracted at 400 °C from fluid inclusions trapped in calcite from syntectonic veins in other, localities kilometers apart, within the Zimapán Basin.

3.1. Clay characterization

Clay separation involved rock crushing, dispersion of powder in de-ionized water in an ultrasonic bath, separation of different clay size-fractions (<0.05 μm, fine; 0.05–0.2 μm, medium-fine; 0.2–1 μm, medium-coarse; 1–2 μm, coarse and <2 μm, bulk clay size-fraction) by centrifugation, and sample drying. Randomly oriented preparations of the <2 μm clay size-fraction samples were created to characterize the mineralogy by scanning from 2°–50° 2θ (Cu Kα) at a rate of 1° per minute. This allowed verification that no other phases containing hydrogen were present in the clay size-fractions. Oriented clay slurry mounts with a concentration of at least 3 mg/cm^2 of the five separated size-fractions were prepared (by sedimentation onto glass slides) and measured from 2 to 30° 2θ under air-dried and glycolated conditions and after heating the samples at 550 °C for 2 hours (Fig. 3). Air-dried and heated samples were measured at a rate of 1°/min, while XRD measurements of glycolated preparations were carried at a speed of 1°/20 seconds. Mineralogical identification, the presence of discrete smectite and smectite, possibly interlayered with illite and/or chlorite, was identified by comparing XRD patterns in air-dried and glycolated preparations as described by Moore and Reynolds (1997). Comparison of peak heights of the basal reflection of 001-kaolinite and 002-chlorite and 002-kaolinite/004-chlorite in air-dried and heated conditions showed the occurrence of kaolinite in the presence of chlorite (Brindley and Brown, 1980). Although these analyses do not permit full clay quantification, they allow identification of discrete and mixed phases, and comparing relative abundances among the different samples.

In order to test temperature of deformation determined from fluid inclusions, we measured the illite crystallinity (IC) or Kübler index (Kübler, 1967 and 1968) of clays. The IC corresponds to the full width ($\Delta 2\theta$ angle) at the half maximum of the 001 basal reflection of the 1 nm peak of illite in the XRD pattern of an oriented preparation, which gives a measure of the ordering/thickness of illite crystallites. This property of illite has been attributed to the temperature of formation (Kübler, 1967 and 1968). Calibration of the IC followed the procedure of Warr and Rice (1994) and temperature estimated considering data reported in Kisch and Merriman (1991), Merriman and Peacor (1999) and Merriman and Frey (1999). Those obtained by fluid inclusion microthermometry, are discussed below.

Scanning Electron Microscopy (SEM) allowed high-resolution optical imaging of textural features of the samples. Minerals and their topographic expression were studied in rock-chips coated with gold and analyzed in the secondary electron mode; mineral phases were analyzed by Energy Dispersive X-ray Spectroscopy (EDS). SEM images showed the distribution of large clay grains (pieces of which could be present in the larger clay size-fractions analyzed) with respect to cleavage or pores fillings.

3.2. Stable isotope analysis

Five size-fractions (bulk, coarse, medium-coarse, fine-medium and fine) from each of the eight shale samples, for a total of 40 aliquots, were analyzed. After air drying, part of the samples were used for XRD characterization and part of them for stable isotope analyses.

Table 2
Composition of analyzed samples, illite crystallinity (IC) and δ^2H and δ^{18}O measured in different clay minerals concentrated in different grain-size fractions: B $\leqslant$ 2 μm, C = 0.2–1 μm, MC = 1–0.2 μm, FM = 0.2–0.05 μm and F $\leqslant$ 0.05 μm (analytical errors are in the order of ±3‰).

Sample	Mineralogy	IC*	δ^2H (‰) VSMOW	δ^{18}O (‰) VSMOW	Sample	Material analyzed/mineralogy	IC*	δ^2H (‰) VSMOW	δ^{18}O (‰) VSMOW
FL1 (B)	Shale, grain size-fraction <2 μm	0.43	−55.1	0.2	BL1 (B)	Shale, grain size-fraction <2 μm	0.48	−76.7	−4.0
FL1 (C)	I, K and traces of Cal and C	0.40	−33.1	3.2	BL1 (C)	S, C/S?, I, K and traces of Cal	0.40	−65.9	−2.2
FL1 (MC)	I, K, Cal and traces of C	0.45	−37.7	7.0	BL1 (MC)	S, C/S?, I and K	0.45	−75.9	−3.4
FL1 (FM)	Cal, I, K and traces of C and S	0.55	−37.7	14.6	BL1 (FM)	S, I/S?, Cal and traces of I	0.60	−66.7	2.7
FL1 (F)	Cal and traces I and K	0.57	−48.7	20.5	BL1 (F)	Cal and traces of I or I/S?	0.50	−43.8	10.5
FL2 (B)	Shale, grain size-fraction <2 μm	0.52	−78.4	9.6	BL2 (B)	Shale, grain size-fraction <2 μm	0.43	−61.8	9.5
FL2 (C)	I and traces of C	0.52	−38.5	3.1	BL2 (C)	Cal, I and C/S?	0.47	−57.6	5.5
FL2 (MC)	I and minor C	0.60	−42.2	1.9	BL2 (MC)	I and traces of Cal, K and C/S?	0.45	−60.1	7.0
FL2 (FM)	Cal, S, I and traces of K	0.65	−53.8	8.7	BL2 (FM)	Cal, I and S	0.60	−57.6	15.9
FL2 (F)	Cal, G and traces of I?	?	−69.5	11.2	BL2 (F)	Cal, I and S?	?	−74.5	21.0
FL3 (B)	Shale, grain size-fraction <2 μm	0.60	−65.2	−3.9	BL3 (B)	Shale, grain size-fraction <2 μm	0.60	−36.2	2.8
FL3 (C)	I, S, C, C/S? And traces of K	0.45	−66	−6.9	BL3 (C)	Cal, I and minor K and C/S	0.52	−65.6	1.0
FL3 (MC)	S, I, C, C/S? and traces of K and Cal	0.55	−67.9	−4.4	BL3 (MC)	I and minor Cal, C and K	0.57	−42	1.4
FL3 (FM)	S, I, C/S? and traces of Cal	0.75	−68	1.4	BL3 (FM)	I and Cal	0.72	−41	5.4
FL3 (F)	S, I and traces of Cal	0.70	−50.5	9.6	BL3 (F)	I and Cal	0.63	−43.7	15.8
FL4 (B)	Shale, grain size-fraction <2 μm	0.64	−75.6	7.9	BL4 (B)	Shale, grain size-fraction <2 μm	0.45	−48	15.4
FL4 (C)	I, S, K and C/S	0.45	−63.9	1.4	BL4 (C)	I, Cal, and minor K	0.50	−47.2	17.2
FL4 (MC)	I, S, C/S and traces of K	0.55	−67.6	1.7	BL4 (MC)	I, K, and traces of Cal	0.55	−45.3	13.9
FL4 (FM)	S, I, C/S? and Cal	0.75	−72.4	5.8	BL4 (FM)	Cal, I and traces of K	0.90	−49.9	15.5
FL4 (F)	Cal, I and S	?	−60.8	14.4	BL4 (F)	Cal and I	0.80	−50.2	20.9

FL stands for fore-limb, or eastern limb, while BL stands for back-limb, samples were collected on the eastern or western limb of assymetrical folds, respectively.

I = illite, Cal = calcite, K = kaolinite, C = chlorite, S = Smectite, I/S = illite/Smectite interlayered, C/S = chlorite-smectite, Qz = quartz, G = Gypsum, IC* = Illite crystallinity calibrated according to Warr and Rice (1994).

In order to verify that no atmospheric water was absorbed on the clay surface prior to isotopic measurements, the samples were first dried at room temperature, and then at 60 °C for 24, 48 and 168 hours in an oven, and were packed in silver capsules. The samples that were dried this way for more than 48 hours showed the best reproducibility and the most positive values, suggesting that atmospheric water adsorbed on clay surface was minimal. Therefore, we repeated this procedure for all samples and measured duplicates in each case. After quickly packing 2–3 mg of dried clay size-fractions in silver capsules, they were immediately measured or temporarily stored in a vacuum line to prevent any atmospheric water adsorption on the silver capsule before their analysis. Because of the temperature conditions of deformation (>200 °C), we targeted discrete illite in this study, which has virtually no interlayered smectite, as confirmed by XRD analyses. We consider that extraction of interlayered water from smectite in a vacuum line prior the analysis of δ^2H of illite unnecessary since, unlike in samples analyzed by Yeh (1980) and Capuano (1992), where illite in most samples was interlayered with smectite, the samples here contain only discrete illite.

The δ^2H and δ^{18}O analyses were done at the Instituto de Geología of the Universidad Nacional Autónoma de México, using a TC/EA reduction unit at 1400 °C with a Conflo III unit as interface to a Finnigan MAT 253 mass spectrometer. Packed samples and silver-packed water standards were pyrolized at 1400 °C in a glassy carbon reaction tube. The gas thus released was separated in a heated GC column and admitted online into the spectrometer along with the international standards (VSMOW, SLAP, GISP and NBS-22 in silver tubes made by the USGS at the Reston Stable Isotope Laboratory) and NBS-22 and IAEA-CH7 in silver capsule, which were analyzed before, during, and after the samples in this study. All isotopic results in this study are reported as permil deviations with respect to the VSMOW-SLAP standard (Coplen, 1988 and 1994).

3.3. Determining the temperature of deformation

Primary fluid inclusions trapped in calcite and quartz from syntectonic veins were selected for microthermometric studies (*e.g.*, Fig. 4 in Fitz-Díaz et al., 2011) by using the petrographic discrimination criteria of Goldstein and Reynolds (1994) and Touret (2001); post-trapping modifications were avoided. All the analyzed fluid inclusions were liquid-rich with neither daughter minerals nor presence of immiscible liquids at room temperature (Fitz-Díaz et al., 2011). Temperatures of homogenization (T_h) and temperatures of ice melting (T_{mi}) were obtained from fluid inclusions by using a Linkam THMSG 600 thermal stage (available at the Instituto de Geología, Universidad Nacional Autónoma de México) that was calibrated with synthetic fluid inclusions, with an estimated analytical precision of ±0.2 °C and ±2 °C at low and high temperature determinations, respectively. The analyzed fluid inclusions corresponded to the H_2O–NaCl system, as suggested by temperatures of melting ice −5.2 to −4.5 °C, a salinity of 8–9 wt.% NaCl equiv., and the isochores were calculated with the equations of state of Bodnar and Vityk (1994) from temperatures of ice melting and temperature of homogenization. The obtained temperatures of homogenization (160–190 °C) correspond to temperatures of trapping between 220 and 250 °C by applying pressure correction (Goldstein and Reynolds, 1994), for which lithostatic conditions (since veins are confined to layers), an average geothermal

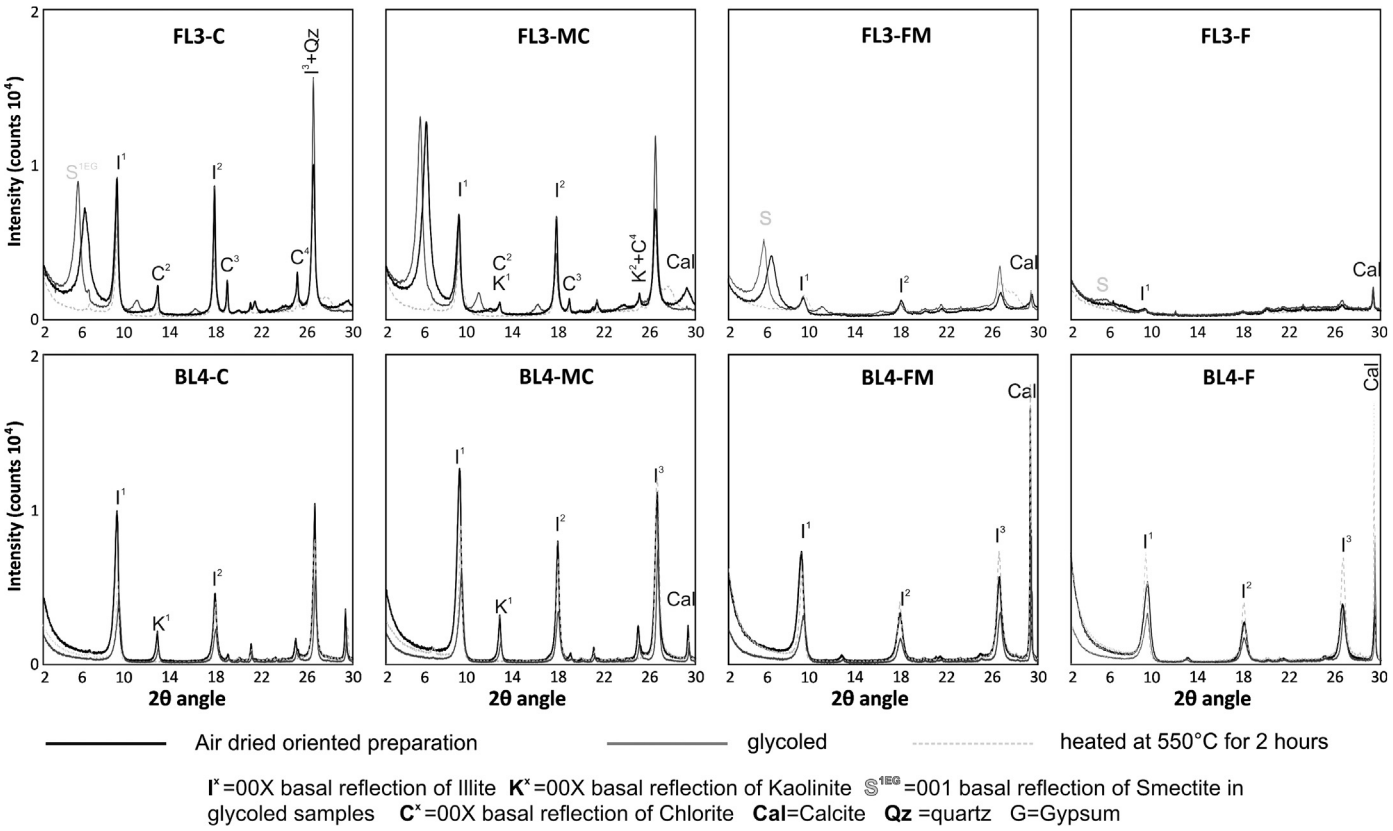

Fig. 3. Examples of XRD patterns of two samples: FL3 is rich in smectite, and BL4 is rich in illite and smectite, and chlorite free. XRD measurements were carried out in oriented preparations of four different clay size-fractions for each sample. Patterns in black correspond to XRD measurements in air-dried samples, grey patterns were obtained after glycolation, and dotted patterns after heating samples at 550 °C for 2 hours. The characteristic basal spectra of clay minerals are indicated in each pattern.

gradient of 28 °C/km in foreland basins (Blackwell et al., 1999) and a geobaric gradient of ~26 MPa/km (assuming an average rock density of 2.7 g/cm^3) were used. This range of temperature is in good agreement with the anchizonal conditions at which the observed illite was formed, supported by illite crystallinity data (*e.g.*, Merriman and Peacor, 1999).

4. Results

4.1. Mineralogical characterization of shale samples

The clay mineral phases that contain H are illite, kaolinite, chlorite and smectite, and occur in samples that also contain calcite and quartz (Table 2). Samples FL1, BL3 and BL4 and BL2 contain illite as the main clay mineral, followed by kaolinite, and in the coarser fraction only recognizable traces of chlorite. BL4 is the only sample where chlorite and smectite are completely absent in all size-fractions (Fig. 3, Annex, Fig. A1). In contrast, samples BL1, FL2, FL3 and FL4 show considerable amounts of smectite and chlorite, particularly concentrated in the coarser fractions (Fig. 3, Fig. A1). In samples FL3, FL4 and BL1, and only in coarser size-fractions of BL2 and BL3 smectite seems to be interlayered with chlorite, according to the shifts observed in the 001 basal reflection of smectite in the air dried and glycolated preparations (Moore and Reynolds, 1997). With exception of finest fractions in BL1, significant shifts in the 001 reflection of illite were observed in the samples, indicating that most of the illite present in the samples is discrete illite (not interlayered with smectite, Moore and Reynolds, 1997). Full mineralogical determinations were not possible in the finest grain size-fraction in most cases, because clay minerals are scarce.

The illite crystallinity index (IC) was determined in 40 oriented preparations, with confident measurements from well-defined peaks of the illite 10 Å reflection in the coarser fractions (<2 μm, coarse and medium coarse) and with lower confidence in the finer fractions (fine-medium and fine). After instrument calibration of measurements using the approach by Warr and Rice (1994), the IC measurements and IC* (calibrated IC) range in the analyzed samples from 0.4 to 0.9$\Delta 2\theta$, generally smaller in the coarser fractions than in the finer fractions (Table 2). The smallest IC* of 0.4 indicates that temperatures of deformation exceeded 200 °C (Kisch and Merriman, 1991; Merriman and Frey, 1999; Merriman and Peacor, 1999), matching the temperatures obtained by microthermometry of fluid inclusions. Four size fractions (<0.05, 0.05–0.2, 0.2–1, and 1–2 μm) from samples BL1 and FL1 were dated with Ar–Ar; only the three coarser fractions of FL1 had sufficient illite and therefore Ar to produce reliable ages in a narrow range between 74.6 and 77.1 Ma (these results are reported in Fitz-Díaz et al., in press, where sample FL1 is coded as SZ3). The facts that (1) all illite ages are younger than rock deposition and contemporaneous to deformation (Fitz-Díaz et al., 2012), (2) the dominant illite polytype (2M1) is consistent with the T of deformation, and (3) well-crystallized illite in the coarser fractions is aligned in the axial plane cleavage, as observed in SEM images (Fig. 4), demonstrate that illite is authigenic.

SEM observations show more porous textures in samples FL2 and FL4 (Fig. 4e, f), containing strongly altered, pseudo-hexagonal illite growing adjacent to altered chlorite. Very small grains of illite–smectite and/or smectite grow as pore-fillings, suggesting that smectite is a product of secondary, late alteration. This is also supported by the fact that smectite is unstable at the measured temperature of deformation (see Fig. 2.1 in Merriman and Peacor, 1999), so it cannot be coeval with discrete 2M1 illite. In contrast, samples BL4 and FL1 (Fig. 4a–d) show relatively large illite grains (2–10 micron in average size) with pseudo-hexagonal

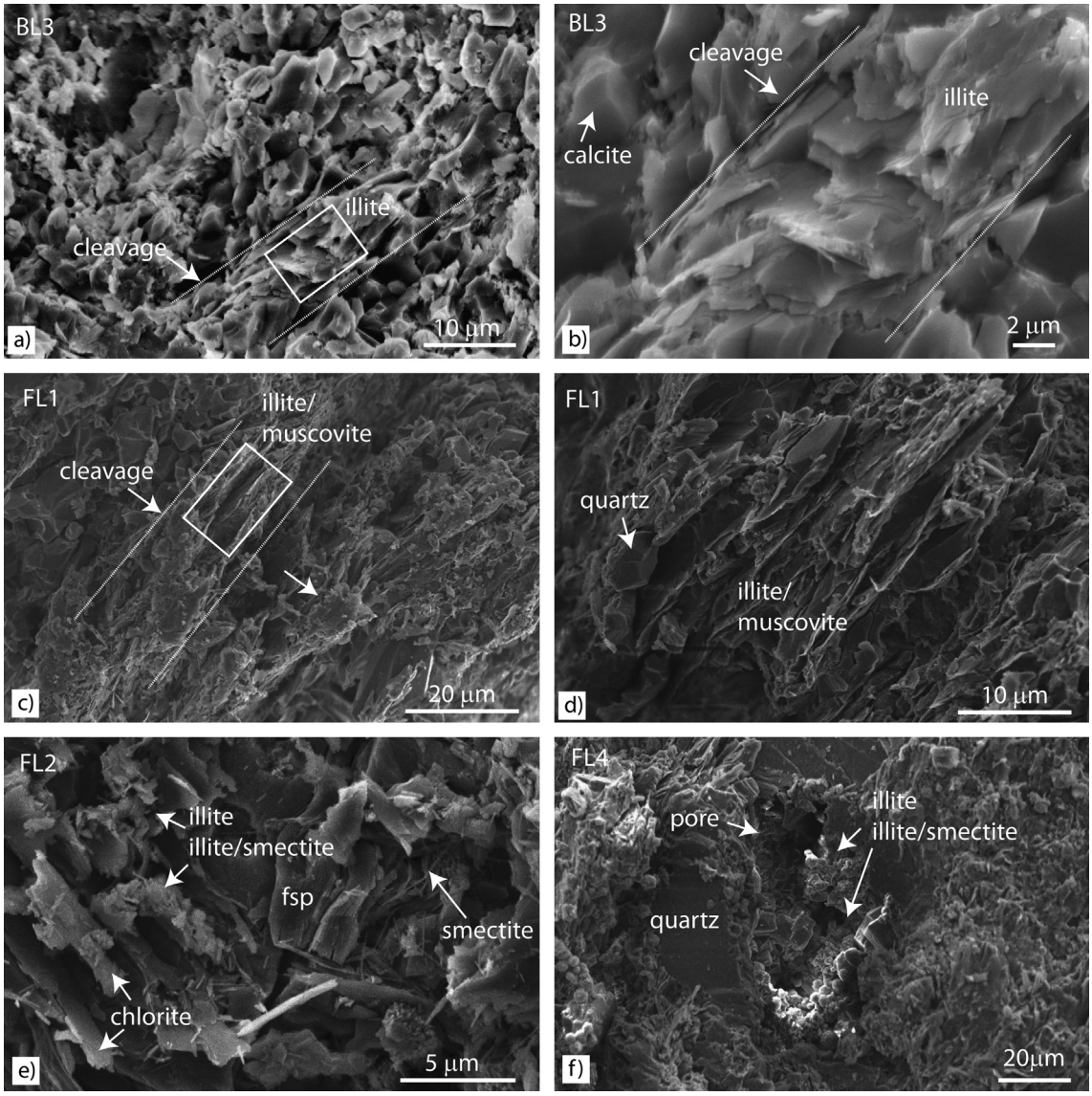

Fig. 4. SEM secondary electron images showing textural aspects of the studied samples: (a) surfaces of BL3 samples showing a homogeneous granular texture and spaced cleavage domains with illite grains oriented parallel; (b) close-up of cleavage domains in (a); (c) pervasive cleavage in FL1 defined by elongate grains of calcite and quartz enveloped by illite grains; (d) close-up of (c); (e) mostly random distribution of illite, smectite and chlorite in the porous shale sample FL2; (f) aspect of a pore in the porous sample FL4.

crystal shapes and some irregular sutured crystal edges, locally defining a homogeneous, anastomosing fabric that is sub-parallel to cleavage domains. Quartz and calcite grains are located between the illite crystals.

4.2. Stable isotope analyses in clay size-fractions

The δ^2H and δ^{18}O values determined in 40 clay concentrates are listed in Table 2. These data constitute average values of duplicate measurements, and these pairs are consistent with the estimated analytical error of ±3‰. The δ^{18}O values vary between −6.9 and 20.9‰, and all samples show the same behavior, with the lowest values in the coarser size-fractions and the highest values in the smallest size-fractions. δ^2H results are as follows: (1) in general, samples with one or two clay phases (*e.g.*, illite and kaolinite) exhibit the best reproducibility (up to 1‰ difference among measurements), (2) samples that contain chlorite and smectite show a poorer reproducibility (within 5‰), and (3) bulk-size-fractions show in general the lowest values (with respect to other size-fractions in the same sample) and the weakest reproducibility (up to 10‰), which probably reflects the mineralogical heterogeneity of these fractions. The exceptions are samples that contain illite as the predominant clay phase, notably the BL4 sample, where isotopic values are close in all size-fractions. For this reason the bulk-size-fractions were excluded from further analyses. Samples with high smectite and chlorite contents show the lowest isotopic values, which range between −75.9 and −53.9‰, whereas illite- and kaolinite-dominated samples show the highest isotopic values, ranging between −33.1 and −50.1‰ (Table 2 and Fig. 5).

5. Discussion

5.1. Reproducibility/reliability of stable isotope data in clay concentrates

We examine δ^2H and δ^{18}O data obtained in each clay size-fraction in the context of mineralogical composition of these samples, from which we make the following observations:

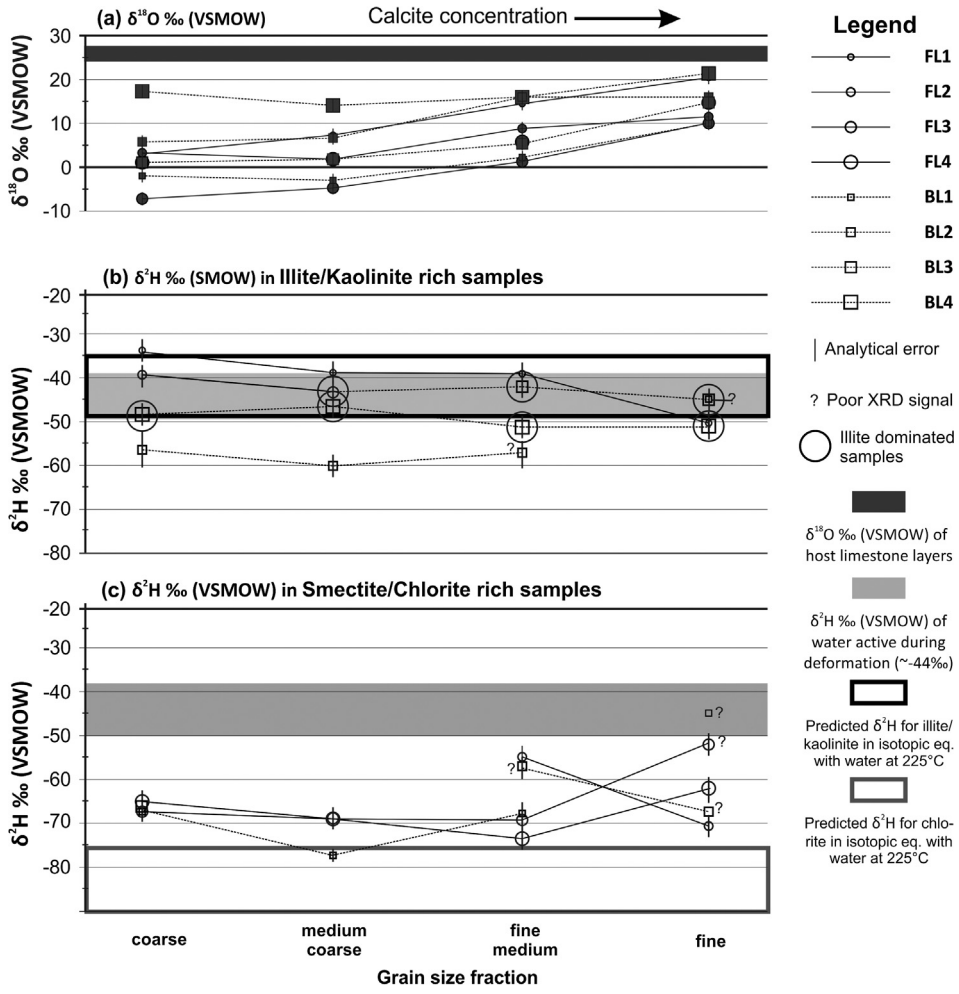

Fig. 5. Stable isotope compositions of clay size-fractions. (a) δ^{18}O measured in four different size-fractions of the eight analyzed samples; note the increase of δ^{18}O as grain size decreases and calcite concentration increases. (b) δ^{2}H size-fraction from samples rich in illite and kaolinite; circled data contain illite as the main clay component; other components (calcite and little quartz) do not affect the δ^{2}H composition. (c) δ^{2}H size-fraction from samples rich in smectite and chlorite. The predicted δ^{2}H values for chlorite and illite in equilibrium with water is about −44‰ at 225 °C, based on the fractionation factors by Graham et al. (1984, 1987) and Hyeong and Capuano (2004).

1) δ^{18}O values vary from −6.9 in calcite-poor samples (coarser fractions) to 20.9‰ in calcite-rich samples (finer size-fractions, Table 2, Fig. 5, and Fig. A1), which is close the 26.4‰ value that corresponds to the average composition of the Cretaceous limestone layers in the study area (Fitz-Díaz et al., 2011). This suggests the role of Cretaceous carbonates in all the analyzed clay concentrates. In addition to calcite, the presence of multiple clay phases and quartz add complexity to the determination of δ^{18}O values for pore water, even when a homogeneous pore water reservoir at the outcrop scale is assumed. Therefore, δ^{18}O data are not able to discriminate the sources of water involved during deformation.
2) The bulk clay size-fractions (<2 μm) show considerable variability and the lowest values in δ^{2}H, which reflects the heterogeneous nature of this fraction and the high contents in chloritic clay, whose fractionation factor in ^{2}H with water differs from that of kaolinite and illite within the relevant temperature range (Fig. 2). Therefore, these data were excluded from further discussion of fluid sources.
3) The smallest clay size-fractions (i.e. 2–1, 1–0.2, 0.2–0.05, and <0.05 μm) yield better mineralogical sorting than merely the clay size-fraction <2 μm; in general, chloritic and smectitic clay are enriched in the coarser fractions, and illitic and kaolinitic clay in the finer fractions. These compositional variations are reflected in the δ^{2}H values, which are higher in the illite- or kaolinite-rich samples, when compared to the chlorite- or smectite-rich samples (Table 2 and Fig. A1) and are in good agreement with predicted δ^{2}H values from the fractionation factors of Lambert and Epstein (1980), Graham et al. (1984 and 1987), and Capuano (1992) for the illite-water, kaolinite-water and chlorite-water systems, respectively (Fig. 2). This indicates that illite, chlorite and kaolinite precipitated from the same fluids and "remember" its isotopic signature.
4) Porous samples (i.e., soft in hand specimen) display the highest content of smectite, reflecting secondary alteration, adding complexity to the interpretation of δ^{2}H values in these samples. Indeed, this later generation of fluids is not likely associated with deformation and shows similar values to local meteoric fluids (Fitz-Díaz et al., 2011).
5) Independent of grain size, samples that show the best reproducibility are compact in hand specimen and contain one or, at most, two clay mineral phases. A good example of this is sample BL4, in which δ^{2}H values from different clay size-fractions (including bulk-size-fraction) are about the same within analytical error. Chlorite-free samples that contain illite and kaolinite, such as the finest fractions of samples of FL1 and BL3, showed similar values to those of sample BL4, thus suggesting that the isotopic composition of kaolinite and illite are very similar. The latter indicates that these minerals precipitated

from the same fluid and "remember" its isotopic signature (see circled data in Fig. 5b, and Table 2).

5.2. Composition of water during deformation

Water trapped in fluid inclusions hosted in calcite and quartz from syn-folding veins was released by decrepitating the fluid inclusions at 100 °C heating steps in a vacuum line (200 to 400 °C in calcite and 300 to 600 °C in quartz) and immediately trapped in Pyrex tubes for δ^2H analyses (Fitz-Díaz et al., 2011). No other fluid that could affect the resulting δ^2H values (*e.g.*, hydrocarbons) was detected or released during this procedure (see Vennemann and O'Neil, 1993). We assume that water released at the lowest temperatures came mostly from fluid inclusions trapped along healed microfractures (secondary inclusions), whereas water released at the highest temperatures (300 to 400 °C in calcite and 500° to 600 °C in quartz) came from pseudosecondary or primary fluid inclusions. The water released from secondary fluid inclusions yields the lowest δ^2H values (as low as −61.2‰), whereas the water released from assumed primary and pseudo-secondary fluid inclusions provides the highest δ^2H values within a consistent range of −41.9 to −45.6‰ (Table 1). Considering the analytical error, we constrain a relatively homogeneous composition for water active during deformation between −39 and −49‰ across the studied outcrop. The fact that secondary fluid inclusions show lower δ^2H values in either case indicates a later passage of fluids with a dominant meteoric water component, which has been previously recorded in other outcrops within the Zimapán Basin and across the Mexican Fold-Thrust Belt (Fitz-Díaz et al., 2011).

The δ^2H values of samples that contain only illite and kaolinite (BL4, BL3 and FL1), and only illite in the finer fractions, vary between −37.7 and −50.2‰, which is in good agreement with the predicted δ^2H compositions for illite and kaolinite considering the composition of water within fluid inclusions. Such prediction accounts for temperatures of deformation between 220 and 250 °C in isotopic equilibrium between water and illite or kaolinite by using the fractionation factors by Capuano (1992) and Lambert and Epstein (1980), respectively (Fig. 2). This indicates that well-preserved illitic clay precipitated in the anchizone from pore water during folding. This is also in good accordance with Ar illite age determinations in sample FL1 of 76.5 ± 1.0 Ma (Fitz-Díaz et al., in press), and the preservation of the δ^2H signature of water involved in deformation. Isotopic equilibrium between authigenic kaolinite and illite with pore water has also been well documented in sedimentary basins during diagenesis (*e.g.*, Longstaffe and Ayalon, 1987 and 1990), and between illite and chlorite and pore water in thrust zones (Lacroix et al., 2012) basins, so we surmise that we are observing the same phenomenon.

5.3. Pore water and folding

Regional folding affecting a heterogeneous package of sedimentary layers (including limestones, shales and cherts) in the middle of the Zimapán Basin in spatially confined conditions, with (1) an elevated pore water pressure (thus allowing fracturing), (2) water–rock interaction (thus promoting pressure solution and material transfer), and (3) restricted fluid flow during folding. These conditions are deduced from the temperature of deformation, the involvement of impermeable shale layers in deformation, the paucity of thrust (as channels for fluid flow), and pervasive pressure-solution cleavage and syntectonic veins in limestone layers across the outcrop. In this scenario, pore water circulation occurs along and across layers through syntectonic fractures/veins, thus allowing a relatively homogeneous composition of the water during deformation at the outcrop scale. This phenomenon of homogenization and compartmentalization of fluid within a horizon has also been observed on kilometer-scale folds (Anastasio et al., 2004; Fischer et al., 2009; Evans and Fischer, 2012; Evans et al., 2012) and is strongly controlled by stratigraphy and the lithological, structural, geochemical and petrological variations of the fluid–rock system. Fluid compartmentalization commonly involves the presence of shale-rich sequences covering a permeable or semipermeable horizon, such as the sequence of Late Cretaceous turbidites covering the Tamaulipas Formation in the Zimapán Basin (Suter, 1987). After removal of the relatively impermeable horizon by erosion, and the subsequent decompression of the rocks underneath, the progressive influx of meteoric fluids into the folded rock assemblage would have been favored. In the studied outcrop, this is supported by lower δ^2H values in secondary than in primary and pseudosecondary fluid inclusions, and by lower δ^2H values in late smectite-rich than in illite- or kaolinite-rich samples.

5.4. Origin and budget of water active during deformation

Given the marine origin of the host rocks, the temperature of deformation, and the absence of contemporaneous magmatism, we identify two possible sources for water during deformation: (a) marine to formational water, and (b) meteoric water, and their mixtures. On one hand, if the fluid source were purely marine, δ^2H values around 0‰ would be expected, according to Eslinger and Yeh (1986) and Compton et al. (1999); on the other hand, for dominantly meteoric sources, δ^2H values between −70 and −60‰ would be expected, as indicated by the composition of water extracted from karst-related late veins in the Zimapán Basin (Fitz-Díaz et al., 2011). Such a range is also similar to that reported for recent meteoric water in Mexico (Wassenaar et al., 2009).

The measured −38 to −50‰ range for δ^2H values in the present study requires a significant involvement of meteoric fluids, as well as remnants of modified marine water, supported by the presence of NaCl–H_2O very diluted brines in fluid inclusions. Specifically, the intermediate δ^2H signature suggests that the meteoric water represented a significant fraction (50% or more) of the active water during deformation. The primary porosity of shale and limestone buried more than 5 km (assuming a surface T of 30 °C and a geothermal gradient of 28 °C/km) represents 5% or less of the total volume (Schmoker and Gautier, 1989), as cementation seals a considerable amount of the original pore volume (Bjørlykke and Hoeg, 1997). Thus, secondary, fold-related fracturing likely increased the porosity of these rocks, following fracture porosity models (*e.g.*, Adams, 2000). The amount of meteoric water that infiltrated the rocks of the Zimapán Basin during deformation probably represented less than 5% of the rock volume, considering that this could have been the maximum pore volume after diagenesis, that pore water is a mixture between formational water (with a δ^2H around 0‰) and meteoric water (with δ^2H as low as −70‰) and that the isotopic composition recorded in illite and water from fluid inclusions is intermediate to those two sources. This scenario of limited fluid and restricted circulation contrasts with the vast amount of circulation through fracture networks that is proposed for ancient (Fisher et al., 1995) and active accretionary fold-thrust wedges (Saffer and Tobin, 2011). However, fluid flow analyses in kilometer-scale folds from structural, fluid inclusions and geochemical analyses in fold-related veins have shown that hydrology during deformation represent a dynamic system (Sibson, 1997; Evans and Battles, 1999; Ferket et al., 2003; Hilgers et al., 2006; Travé et al., 2007; Fitz-Díaz et al., 2011; Evans and Fischer, 2012). It involves cycles of compression and relaxation during which fracturing/veining can occur, thus facilitating fluid infiltration through repeatedly evolving fracture networks. Some studies have also shown that stylolites and pressure-solution seams allow fluid flow along them (Bjørlykke, 1997; Deschamps et al., 2004), although fluid circulation through interconnected

fractures/veins and stylolites or pressure-solution cleavage domains is not as efficient in allowing fluid flow as major faulting.

6. Conclusions

We use an integrated approach to study fluid source(s) in deformed basinal sequences of northern mexico, including: (1) δ^2H values of water trapped in fluid inclusions of syn-folding veins, (2) δ^2H values of structural water of syn-folding illite in the same train of mesoscopic folds, which are consistent with δ^2H values in inclusion fluids, (3) H isotope fractionation factors between illite and water and well-constrained temperatures of deformation, (5) salinity data from fluid inclusions microthermometry, (6) Ar–Ar illite geochronology, which shows that illite was coeval with local deformation, and (7) XRD based mineralogical data that allow discrimination between samples containing only discrete illite from those containing multiple clay minerals. The results show that discrete illite, formed in anchizonal bentonitic shale, is able to preserve the isotopic composition of water from which it precipitated during deformation. The fractionation factor of ^{2}H between illite and water of Capuano (1992), which considers isotopic data from illite under geopressurized conditions, works well for illite that precipitated between 220 and 250 °C. The fractionation factor by Yeh (1980), on the other hand, underestimates the ^{2}H content in illite with respect to water.

By applying our methodology to illite in folded layers of the Mexican Fold-Thrust Belt we are able to constrain δ^2H values between −38 and −50‰ for pore water active during their formation in the Zimapán Basin. This suggests a homogeneous fluid reservoir at the outcrop scale, which, based on fluid inclusion studies, contained formational brines. Deformation occurred at temperatures that range from 220 to 250 °C, as determined from microthermometry of fluid inclusions and the crystallinity index of neoformed illite. The system was proportionally affected by meteoric water inflow, likely through an evolving, dynamically-connected pore, fracture and stylolite/cleavage network during folding. Contrary to studies in accretionary prisms, where fluid active during deformation represents multiples of the rock volume, the amount of fluid that was active during deformation in these rocks only represents a fraction of the rock volume. Combined with high pore fluid pressure, this suggests productive rock/water interaction and reuse/recycling of pore water during pressure-solution and material transfer associated with regional deformation.

Acknowledgements

We thank Francisco Otero for his careful assistance during the preparation of the samples and three reviewers for their thoughtful comments that significantly improved the paper. Research was supported by a U-M Turner Postdoctoral Fellowship to Elisa Fitz-Díaz, National Science Foundation grants EAR 1118704 and 1216750 (to BvdP), and CONACYT (Mexican Government) grant 155662 (to AC).

Appendix A. Supplementary material

Supplementary material related to this article can be found online at http://dx.doi.org/10.1016/j.epsl.2013.12.025.

References

Adams, S.J., 2000. Fracture porosity from conventional logs with image tool calibration. In: SPE Asia Pacific Oil and Gas Conference and Exhibition.

Anastasio, D.J., Bebout, G.E., Holl, J.E., 2004. Extra-basinal fluid infiltration, mass transfer, and volume strain during folding; insights from the Idaho–Montana thrust belt. Am. J. Sci. 304, 333–369.

Bjørlykke, K., 1997. Lithological control on fluid flow in sedimentary basins. In: Jamtveit, B., Yardley, B. (Eds.), Fluid Flow and Transport in Rocks: Mechanisms and Effects. Chapman and Hall, Oxford, UK, pp. 15–34.

Bjørlykke, K., Hoeg, K., 1997. Effects of burial diagenesis on stresses, compaction and fluid flow in sedimentary basins. Mar. Petroleum Geol. 14, 267–276.

Bodnar, R.J., Vityk, M.O., 1994. Interpretation of microthermometric data for H_2O–NaCl fluid inclusions. In: De Vivo, B., Frezzotti, M.L. (Eds.), Fluid Inclusions in Minerals, Methods and Applications. Virginia Tech, Blacksburg, VA, pp. 117–130.

Blackwell, D.D., Richards, M., Wisian, K.W., Steele, J.L., Johnson, Stuart D., et al., 1999. System specific geothermal gradient/heat flow data base for the Western United States. Trans., Geotherm. Resour. Counc. 23, 461–466.

Brindley, G.W., Brown, G., 1980. Crystal Structures of Clay Minerals and Their X-Ray Identification. Mineral Soc., London, UK.

Capuano, R.M., 1992. The temperature dependence of hydrogen isotope fractionation between clay minerals and water: Evidence from a geopressured system. Geochim. Cosmochim. Acta 56, 2547–2554.

Chacko, T., Cole, D.R., Horita, J., 2001. Equilibrium oxygen, hydrogen and carbon isotope fractionation factors applicable to geologic systems: Stable isotope geochemistry. Rev. Mineral. Geochem. 43, 1–81.

Compton, J.S., Conrad, M.E., Vennemann, T.W., 1999. Stable isotope evolution of volcanic ash layers during diagenesis of the Miocene Monterey formation, California. Clays Clay Miner. 47, 84–95.

Coplen, T.B., 1988. Normalization of oxygen and hydrogen isotope data. Chem. Geol. (Isot. Geosci. Sect.) 72, 293–297.

Coplen, T.B., 1994. Reporting of stable hydrogen, carbon, and oxygen isotopic abundances. Pure Appl. Chem. 66, 273–276.

Cosgrove, J.W., 1993. The interplay between fluids, folds and thrusts during the deformation of a sedimentary succession. J. Struct. Geol. 15, 491–500.

Deschamps, P., Hillaire-Marcel, C., Michelot, J.L., Doucelance, R., Ghaleb, B., 2004. ^{234}U/^{238}U disequilibrium along stylolitic discontinuities in deep Mesozoic limestone formations of the eastern Paris Basin; evidence for discrete uranium mobility over the last 1–2 million years. Hydrol. Earth Syst. Sci. 8, 35–46.

Durney, D.W., 1972. Solution-transfer, an important geological deformation mechanism. Nature 235, 315–317.

Engelder, T., 1984. The role of pore water circulation during the deformation of Foreland Fold and Thrust Belts. J. Geophys. Res. 89, 4319–4325.

Eslinger, E.V., Yeh, H., 1986. Oxygen and hydrogen isotope geochemistry of Cretaceous bentonites and shales from the Disturbed Belt, Montana. Geochim. Cosmochim. Acta 50, 59–68.

Eslinger, E.V., Savin, S.M., Yeh, H.W., 1979. Oxygen isotope geothermometry of diagenetically altered shales. Spec. Publ., Soc. Econ. Paleontol. Mineral. 26, 113–124.

Evans, M.A., Battles, D.A., 1999. Fluid inclusion and stable isotope analysis of veins from the central Appalachian Valley and Ridge province: implications for regional synorogenic hydrologic structure and fluid migration. Geol. Soc. Am. Bull. 111, 1841–1860.

Evans, M.A., Fischer, M.P., 2012. On the distribution of fluids in folds: A review of controlling factors and processes. J. Struct. Geol. 44, 2–24.

Evans, M.A., Bebout, G.E., Brown, C.H., 2012. Changing fluid conditions during folding: An example from the central Appalachians. Tectonophysics 577–578, 99–115.

Ferket, H., Swennen, R.A.J., Ortuño, S., Roure, F., 2003. Reconstruction of the fluid flow history during Laramide foreland folds and thrust belt development in eastern Mexico; cathodoluminescence and δ^{18}O–δ^{13}C isotope trends of calcite-cemented fractures. J. Geochem. Explor. 78–79, 163–167.

Fischer, M.P., Higuera-Diaz, I.C., Evans, M.A., Perry, E.C., Lefticariu, L., 2009. Fracture-controlled paleohydrology in a map-scale detachment fold; insights from the analysis of fluid inclusions in calcite and quartz veins. J. Struct. Geol. 31, 1490–1510.

Fisher, D.M., Brantley, S.L., Everett, M., Dzvonik, J., 1995. Cyclic fluid flow through a regionally extensive fracture network within the Kodiak accretionary prism. J. Geophys. Res. B 7 (12), 881–894.

Fitz-Díaz, E., Tolson, G., Camprubí, A., Rubio-Ramos, M.A., Prol-Ledesma, R.M., 2008. Deformación, vetas, inclusiones fluidas y la evolución tectónica de las rocas cretácicas de Valle de Bravo, Estado de México, México. Rev. Mex. Cienc. Geol. 25, 59–81.

Fitz-Díaz, E., Hudleston, P., Kirschner, D., Siebenaller, L., Camprubí, A., Tolson, G., Pi-Puig, T., 2011. Insights into fluid flow and water–rock interaction during deformation of carbonate sequences in the Mexican fold-thrust belt. J. Struct. Geol. 33, 1237–1253.

Fitz-Díaz, E., Tolson, G., Hudleston, P., Bolaños-Rodriguez, D., Ortega-Flores, B., Vázquez-Serrano, A.V., 2012. The role of folding in the development of the Mexican fold-and-thrust belt. Geosphere 8, 931–949.

Fitz-Díaz, E., Hudleston, P.J., Tolson, G., van der Pluijm, B., in press. Progressive deformation in the Mexican Fold-Thrust Belt (Central México): evidence from radiometric dating of folds and faults. Geosphere.

Foreman, J.L., Dunne, W.M., 1991. Conditions of vein formation in the Southern Appalachian foreland; constraints from vein geometries and fluid inclusions. J. Struct. Geol. 13, 1173–1183.

Fyfe, W.S., Kerrich, R., 1985. Fluids and thrusting. Chem. Geol. 49, 353–362.

Goldstein, R.H., Reynolds, T.J., 1994. Systematics of fluid inclusions in diagenetic minerals. In: SEPM Short Course Notes, vol. 31, p. 199.

Graham, C.M., Atkinson, J., Harmon, R.S., 1984. Hydrogen isotope fractionation in the system chlorite-water. Prog. Exp. Petrol. 6, 139–140.
Graham, C.M., Viglino, J.A., Harmon, R.S., 1987. Experimental study of hydrogen-isotope exchange between aluminous chlorite and water and of hydrogen diffusion in chlorite. Am. Mineral. 72, 566–579.
Hilgers, C., Kirschner, D.L., Breton, J.P., Urai, J.L., 2006. Fracture sealing and fluid overpressures in limestones of the Jabal Akhdar Dome, Oman Mountains. Geofluids 6, 168–184.
Hodgkins, M.A., Stewart, K.G., 1994. The use of fluid inclusions to constrain fault zone pressure, temperature and kinematic history; an example from the Alpi Apuane, Italy. J. Struct. Geol. 16, 85–96.
Hubbert, M.K., Rubey, W.W., 1959. Role of fluid pressure in mechanics of overthrust faulting. I. Mechanics of fluid-filled porous solids and its application to overthrust faulting. Geol. Soc. Am. Bull. 70, 115–166.
Hudleston, P.J., 1989. The association of folds and veins in shear zones. J. Struct. Geol. 11, 949–957.
Hyeong, K., Capuano, R.M., 2004. Hydrogen isotope fractionation factor for mixed-layer illite/smectite at 60° to 150 °C; new data from the northeast Texas Gulf Coast. Geochim. Cosmochim. Acta 68, 1529–1543.
James, A.T., Baker, D.R., 1976. Oxygen isotope exchange between illite and water at 22 °C. Geochim. Cosmochim. Acta 40, 235–239.
Kirschner, D.L., Kennedy, L.A., 2001. Limited syntectonic fluid flow in carbonate-hosted thrust faults of the Front Ranges, Canadian Rockies, inferred from stable isotope data and structures. J. Geophys. Res. 106, 8827–8840.
Kisch, H.J., Merriman, R.J., 1991. Development of slaty cleavage and degree of very-low-grade metamorphism; a review. J. Metamorph. Geol. 6, 735–750.
Kübler, B., 1967. La cristallinité de l'illite et les zones tout à fait supérieures du metamorphisme. In: Étages tectoniques. Colloque de Neuchâtel. 18–21 avril 1966. Université de Neuchâtel, Institut de Géologie, pp. 105–122.
Kübler, B., 1968. Évaluation quantitative du métamorphisme par la cristallinité de l'illite; état des progrès realisés ces dernières années. Bull. Cent. Rech., Pau (Soc. Nat. Pet. Aquit.) 2, 385–397.
Lacroix, B., Buatier, M., Labaume, P., Travé, A., Dubois, M., Charpentier, D., Ventalon, S., Convert-Gaubier, D., 2011. Microtectonic and geochemical characterization of thrusting in a foreland basin: example of the south-Pyrenean orogenic wedge (Spain). J. Struct. Geol. 33, 1359–1377.
Lacroix, B., Charpentier, D., Buatier, M., Vennemann, T., Labaume, P., Adatte, T., Travé, A., Dubois, M., 2012. Formation of chlorite during thrust fault reactivation. Record of fluid origin and P–T conditions in the Monte Perdido thrust fault (southern Pyrenees). Contrib. Mineral. Petrol. 163, 1083–1102.
Lambert, S.J., Epstein, S., 1980. Stable isotope investigations of an active geothermal system in Valles Caldera, Jemez mountains, New Mexico. J. Volcanol. Geotherm. Res. 8, 111–129.
Longstaffe, F.J., Ayalon, A., 1987. Oxygen-isotope studies of clastic diagenesis in the Lower Cretaceous Viking Formation, Alberta: implications for the role of meteoric water implications for the role of meteoric water. Geol. Soc. (Lond.) Spec. Publ. 36, 277–296.
Longstaffe, F.J., Ayalon, A., 1990. Hydrogen-isotope geochemistry of diagenetic clay minerals from Cretaceous sandstones, Alberta, Canada: evidence for exchange. Appl. Geochem. 5, 657–668.
Marshak, S., Engelder, T., 1984. Development of cleavage in limestones of a fold-thrust belt in Eastern New York. J. Struct. Geol. 7, 345–359.
Merriman, R.J., Frey, D., 1999. Patterns of very-low grade metamorphism in metapelitic. In: Frey, M., Robinson, D. (Eds.), Low-Grade Metamorphism. Blackwell Science, UK, pp. 91–107.
Merriman, R.J., Peacor, D.R., 1999. Very-low grade metapelites: mineralogy, microfabrics and measuring reaction progress. In: Frey, M., Robinson, D. (Eds.), Low-Grade Metamorphism. Blackwell Science, UK, pp. 10–60.
Moore, D.M., Reynolds Jr., R.C., 1997. X-ray Diffraction and the Identification and Analysis of Clay Minerals. Oxford University Press, Oxford, United Kingdom.
Ramsay, J.G., 1967. Folding and Fracturing of Rocks. McGraw–Hill, New York.
Richards, I., Connelly, J., Gregory, R., Gray, D., 2002. The importance of diffusion, advection, and host-rock lithology on vein formation: A stable isotope study from the Paleozoic Ouachita orogenic belt, Arkansas and Oklahoma. Geol. Soc. Am. Bull. 114, 1343–1355.
Rutter, E.H., 1983. Pressure solution in nature, theory and experiment. J. Geol. Soc. 140, 725–740.
Rye, D.M., Bradbury, H.J., 1988. Fluid flow in the crust: an example from a Pyrenean thrust ramp. Am. J. Sci. 288, 197–235.
Saffer, D.M., Tobin, H.J., 2011. Hydrogeology and mechanics of subduction zone forearcs: Fluid flow and pore pressure. Annu. Rev. Earth Planet. Sci. 39, 157–186.
Savin, S.M., Epstein, S., 1970. The oxygen and hydrogen isotope geochemistry of clay minerals. Geochim. Cosmochim. Acta 34, 25–42.
Schmoker, J.W., Gautier, D.L., 1989. Compaction of basin sediments; modeling based on time-temperature history. J. Geophys. Res. 94, 7379–7386.
Sibson, R.H., 1997. Selective fault reactivation during basin inversion: potential for fluid redistribution through fault-valve action. Geol. Soc. (Lond.) 88, 3–19.
Sheppard, S.M.F., Gilg, H.A., 1996. Stable isotope geochemistry of clay minerals. Clay Miner. 31, 1–24. http://dx.doi.org/10.1180/claymin.1996.031.1.01.
Suter, M., 1987. Structural traverse across the Sierra Madre Oriental fold-thrust belt in east-central Mexico. Geol. Soc. Am. Bull. 98, 249–264.
Touret, J.L.R., 2001. Fluids in metamorphic rocks. Lithos 55, 1–25.
Travé, A., Labaume, P., Vergés, J., 2007. Fluid systems in foreland fold-and-thrust belts: an overview from the southern Pyrenees. In: Lacombe, O., Lave, J., Roure, F., Vergés, J., Brun, J.P., Oncken, O., Weissert, H., Dullo, C. (Eds.), Thrust Belts and Foreland Basins. From Fold Kinematics to Hydrocarbon Systems. Springer.
Vennemann, T.W., O'Neil, J.R., 1993. A simple and inexpensive method of hydrogen isotope and water analyses of minerals and rocks based on zinc reagent. Chem. Geol. 103, 227–234.
Warr, L.N., Rice, A.H.N., 1994. Interlaboratory standardization and calibration of clay mineral crystallinity and crystallite size data. J. Metamorph. Geol. 12, 141–152.
Wassenaar, L.I., van Wilgenburg, S.L., Larson, K., Hobson, K.A., 2009. A groundwater isoscape (δD, δ^{18}O) for Mexico. In: Isoscapes: Isotope Mapping and Its Applications. J. Geochem. Explor. 102, 123–136.
Yeh, H.W., 1980. D/H ratios and late-stage dehydration of shales during burial. Geochim. Cosmochim. Acta 44, 341–352.